[Ru(bpy)$_2$(Meimpy)]Br$_2$, 87306-10-3; (+)-[Ru(bpy)$_2$(Meimpy)](Sb$_2$(+)tart$_2$), 87334-87-0; (+)-[Ru(bpy)$_2$(Meimpy)](PF$_6$)$_2$, 87334-88-1; Λ-(+)-[Ru(bpy)$_2$((*S*)(−)-Meampy)]$^{2+}$, 87334-89-2; Δ-(−)-[Ru(bpy)$_2$((*S*)(−)-Meampy)]$^{2+}$, 87334-90-5; Ru(bpy)$_2$(ampy)$^{2+}$, 56889-71-5; deuterium, 7782-39-0.

Supplementary Material Available: Tables of thermal parameters for the non-hydrogen atoms (Supplementary Table 1), calculated positional parameters for the hydrogen atoms (Supplementary Table 2), and observed and calculated structure factors (Supplementary Table 3) for the structure determination (16 pages). Ordering information is given on any current masthead page.

Chemical Reaction Paths. 9. Conformational Interconversions of Wilkinson's Catalyst and of Related Square-Planar XM(PR$_3$)$_3$ Compounds As Determined from Systematic Analysis of Solid-State Structural Data[1,2]

K. Chandrasekhar and Hans-Beat Bürgi*

Contribution from the Laboratorium für chemische und mineralogische Kristallographie der Universität, CH-3012 Bern, Switzerland. *Received March 1, 1983*

Abstract: Structural data on 15 independent molecules of the type XM(PR$_3$)$_3$ (X = H$^-$, F$^-$, CO_3^{2-}, Cl$^-$; M = Rh(I), Pt(II); R = CH_3, CH_2CH_3, $CH(CH_3)_2$, C_6H_5) have been retrieved from the Cambridge Structural Database. The conformation of each molecule has been characterized by torsion angles about the M–P bonds, one for each of the three PR$_3$ groups. The symmetry of the molecules has been analyzed in terms of a group of order 108. The analysis is based on a nonrigid molecular model of three C_{3v}-symmetric rotors PR$_3$ on a C_{2v}-symmetric frame XMP$_3$. The 15 sets of 108 symmetry-equivalent conformations are not distributed randomly in the space defined by the three torsion angle coordinates but delineate two distinct pathways of conformational interconversion. The changes in conformation along one of them may be described in terms of a simple mechanical analogy, namely gearing motion of three interlocked cogwheels. Along the other, the analogy is to gearing motion on one side of the central PR$_3$ group and to gear slippage on the other. The observed changes of the C–P–M bond angles are related to changes in torsion angles about the M–P bonds and so are the changes in the nonplanarity of the XMP$_3$ frame. The analysis exemplifies possible mechanisms for transmission of structural information from one side of a metal complex to the other as is postulated for asymmetric hydrogenation catalysts. Implications of the analysis on the relationship between structure in the solid state and in solution are also discussed.

1. Introduction

Crystal structure determinations for square-planar molecules of the type XM(PR$_3$)$_3$ (Figure 1) include examples with M = Rh(I), Pt(II), X = H$^-$, CO_3^{2-}, F$^-$, Cl$^-$, and R = CH_3, CH_2CH_3, $CH(CH_3)_2$, C_6H_5.[3-13] Such molecules show a bewildering variety of conformations, a wide variation in R–P–M and P–M–P bond angles, and XMP$_3$ skeletons, which are sometimes planar and sometimes not (Table I). Of course, one could argue that structural detail in these complexes depends on the chemical nature of R, X, and M and that understanding these structures requires an understanding of the individual interactions in these molecules. We have chosen a different viewpoint, however: All XM(PR$_3$)$_3$ molecules are considered to contain the same basic molecular fragment, namely XM(PC$_3$)$_3$, which is essentially square planar with X–M–P, P–M–P, and C–P–M bond angles of 80 ± 10°, 100 ± 10°, and 117 ± 13°, respectively. We are not interested in the detailed effects of a particular M, X, or R on an individual molecular structure. We rather want to analyze whether or not there is an overall pattern in the observed conformations and other structural parameters. In this approach the chemical nature of M, X, and R is not important by itself, it merely takes the part of a structural perturbation that serves to probe the flexibility of the molecular fragment of interest.[14,15] This viewpoint has enabled us to perform a detailed conformational analysis of XM(PR$_3$)$_3$ molecules and to delineate the effects of conformational changes on bond angles and the planarity of the XMP$_3$ skeleton. Indispensable tools for an efficient analysis turn out to be (1) The Cambridge Structural Database (CSD),[16] (2) the concept of symmetry of nonrigid molecules,[17,18] and (3) statistical methods.[19]

(1) Dedicated to Prof. Dr. Jack D. Dunitz on the occasion of his 60th birthday, in remembrance of past collaborative efforts in this series (ref 2b).

(2) (a) Part 8: Bye, E.; Schweizer, W. B.; Dunitz, J. D. *J. Am. Chem. Soc.* **1982**, *104*, 5893. (b) Part 2: Bürgi, H. B.; Dunitz, J. D.; Shefter, E. *Ibid.* **1973**, *95*, 5065. Part 4: Bürgi, H. B.; Dunitz, J. D.; Shefter, E. *Acta Crystallogr., Sect. B* **1974**, *B30*, 1517. Part 5: Murray-Rust, P.; Bürgi, H. B. Dunitz, J. D. *J. Am. Chem. Soc.* **1975**, *97*, 921. Part 6: Bürgi, H. B.; Shefter, E.; Dunitz, J. D. *Tetrahedron* **1975**, *31*, 3089.

(3) Russell, D. R.; Mazid, M. A.; Tucker, P. A. *J. Chem. Soc. Dalton Trans.* **1980**, 1737.

(4) Strauss, S. H.; Diamond, S. E.; Mares, F.; Shriver, D. F. *Inorg. Chem.* **1978**, *17*, 3064.

(5) Caputo, R. E.; Mak, D. K.; Willett, R. D.; Roundhill, S. G. N.; Roundhill, D. M. *Acta Crystallogr., Sect. B* **1977**, *B33*, 215.

(6) Gusev, A. I.; Struchkov, Yu. T. *Zh. Strukt. Khim.* **1974**, *15*, 282.

(7) Favez, R.; Roulet, R.; Pinkerton, A. A.; Schwarzenbach, D. *Inorg. Chem.* **1980**, *19*, 1356.

(8) Jones, R. A.; Real, F. M.; Wilkinson, G.; Galas, A. M. R.; Hursthouse, M. B. *J. Chem. Soc., Dalton Trans.* **1981**, 126.

(9) Yoshida, T.; Thorn, D. L.; Okano, T.; Otsuka, S.; Ibers, J. A. *J. Am. Chem. Soc.* **1980**, *102*, 6451.

(10) Krogsrud, S.; Komiya, S.; Ito, T.; Ibers, J. A.; Yamamoto, A. *Inorg. Chem.* **1976**, *15*, 2798.

(11) Hitchcock, P. B.; McPartlin, M.; Mason, R. *J. Chem. Soc., Chem. Commun.* **1969**, 1367.

(12) Bennett, M. J.; Donaldson, P. B. *Inorg. Chem.* **1977**, *16*, 655.

(13) Jones, R. A.; Real, F. M.; Wilkinson, G.; Galas, A. M. R.; Hursthouse, M. B.; Abdul Malik, K. M. *J. Chem. Soc., Dalton Trans.* **1980**, 511.

(14) This is a paraphrase of the principle of structural correlation. Murray-Rust, P.; Bürgi, H. B.; Dunitz, J. D. *J. Am. Chem. Soc.* **1975**, *97*, 921.

(15) Dunitz, J. D. "X-Ray Analysis and the Structure of Organic Molecules"; Cornell University Press: Ithaca, NY, 1979; p 363.

(16) Allen, F. H.; Bellard, S.; Brice, M. D.; Cartwright, B. A.; Doubleday, A.; Higgs, H.; Hummelink, T.; Hummelink-Peters, B. G.; Kennard, O.; Motherwell, W. D. S.; Rogers, J. R.; Watson, D. G. *Acta Crystallogr., Sect. B* **1979**, *B35*, 2331.

(17) Longuet-Higgins, H. C. *Mol. Phys.* **1963**, *6*, 445.

(18) Frei, H.; Bauder, A.; Günthard, H. H. *Topics Current Chemistry* **1979**, *81*, 3.

0002-7863/83/1505-7081$01.50/0

Table 1. Selected Bond Angles α, Torsion Angles ω, and Other Geometrical Parameters for 15 Molecules of the Type $XM(PR_3)_3$[a]

compd	α_{11}	α_{12}	α_{13}	α_{21}	α_{22}	α_{23}	α_{31}	α_{32}	α_{33}	α_{1M_2}	α_{3M_2}	α_{1M_3}	δ[b]	d[c]
1	121.4	109.4	108.9	118.2	113.8	113.9	118.3	108.7	113.3	100.1	101.5	158.4	0.6	3.55
2	124.8	109.9	115.0	118.9	119.3	110.3	119.1	115.7	115.5	102.3	104.0	151.7	6.5	3.35
3	112.1	109.6	125.2	119.4	107.6	115.9	116.2	110.6	113.0	101.0	99.5	159.5	1.0	3.46
4	117.1	110.9	117.7	108.4	120.8	120.8	118.3	106.0	124.9	96.6	98.5	161.3	6.4	3.44
5	104.5	115.9	126.7	111.6	115.3	120.4	113.5	107.3	125.4	100.1	94.5	160.8	7.2	3.17
6	110.5	114.3	128.3	111.5	114.7	121.9	111.4	112.6	126.4	100.7	93.3	165.9	1.1	3.23
7	124.2	109.2	113.0	119.0	112.6	110.9	121.2	110.8	110.3	101.2	103.7	155.2	0.5	3.30
8	108.7	110.2	125.2	120.1	110.9	111.7	125.9	110.6	108.3	95.6	101.6	162.6	1.6	3.18
9	125.3	109.3	112.2	113.8	117.9	116.7	126.4	109.4	110.5	109.2	109.3	141.5	0.5	3.52
10	123.2	107.8	118.3	108.0	123.2	112.4	129.7	113.6	108.3	99.7	96.0	151.1	14.0	3.30
11	124.5	105.5	118.6	114.5	118.7	111.4	119.6	106.1	121.8	96.3	96.6	154.4	12.4	3.20
12	122.3	104.5	120.7	119.1	116.3	110.0	114.2	112.7	123.4	96.5	97.7	159.1	8.8	3.22
13	118.4	112.9	120.4	114.0	121.8	118.6	115.9	113.2	122.4	95.7	94.7	164.0	6.8	3.63
14	118.7	109.6	115.3	111.3	114.5	117.3	113.4	109.0	121.7	98.6	95.0	165.6	2.8	3.53
15	121.2	104.2	121.6	114.1	123.5	109.8	117.1	107.3	124.6	97.8	100.4	152.9	11.9	3.44
	ω_{11}	ω_{12}	ω_{13}	ω_{21}	ω_{22}	ω_{23}	ω_{31}	ω_{32}	ω_{33}	ω_1[b]	ω_2[b]	ω_3[b]	P[b]	M[d]
1	3.7	129.8	238.1	89.5	209.5	327.3	51.9	173.1	292.9	3.9	88.8	52.6	0.24	4, 5
2	7.0	126.6	240.7	58.7	182.4	303.0	81.4	203.1	321.8	4.8	61.4	82.1	0.10	4, 5
3	116.2	229.6	354.1	102.1	223.4	343.3	75.7	188.9	305.1	113.3	102.9	69.9	0.22	4, 5
4	65.6	177.6	295.9	42.2	163.1	289.1	105.2	221.2	337.6	59.7	44.8	101.3	0.16	6, 7
5	113.9	229.7	357.3	38.0	160.0	280.7	121.2	237.1	353.9	113.6	39.6	117.4	0.23	6, 7
6	111.2	226.4	350.2	36.8	157.8	278.6	117.5	233.5	355.9	109.3	37.7	115.6	0.25	6, 7
7	2.5	130.6	234.5	95.5	219.5	335.3	25.3	151.4	260.5	2.5	96.8	25.7	0.17	4, 5
8	121.1	237.7	359.9	87.6	204.4	326.9	0.3	124.5	238.1	119.6	86.3	1.0	0.24	4, 5
9	7.2	133.8	246.0	42.0	161.4	278.7	3.0	130.9	242.4	9.0	40.7	5.4	0.21	6, 7
10	10.9	127.5	240.5	49.5	172.5	299.1	11.2	135.9	251.7	6.3	53.7	12.9	0.20	6, 7
11	4.5	124.3	238.4	54.5	180.3	304.6	106.9	225.4	339.5	2.4	59.8	103.9	0.12	6, 7
12	17.6	133.0	249.6	63.7	188.6	312.8	112.9	231.2	348.9	13.4	68.4	111.0	0.13	4, 5
13	48.6	163.6	282.3	48.4	171.2	295.6	92.5	209.6	326.4	44.8	51.7	89.5	0.06[e] −0.02	4-7
14	51.7	167.4	283.4	42.2	162.3	284.2	91.1	207.7	326.6	47.5	42.9	88.5	0.09[e] −0.01	4-7
15	25.3	138.0	256.2	54.5	179.9	303.3	106.4	221.5	338.1	19.8	59.2	102.0	0.01[e] 0.06	4-7

[a] α's, ω's, δ are in degrees, d in Å, and p is dimensionless. Chemical name (CSD reference code and literature reference number) for compounds 1–15. 1, 7: hydridotris(triethylphosphine)platinum(II) hexafluorophosphate (TEPPTA, 3). 2: hydridotris(triphenylphosphine)-rhodium(I) dimethylamine solvate tetrahydrofuran solvate (HTPRHS, 4). 3: hydridotris(triphenylphosphine)platinum(II) hydrogen bis(trifluoroacetate) (HPTFAC, 5). 4: (benzoato)tris(triphenylphosphine)rhodium(I) benzene solvate (TPRHBZ, 6). 5: chlorotris(trimethylphosphine)platinum(II) chloride (CMPHPT, 7). 6: *trans*-chlorobis(trimethylphosphine)(triphenylphosphine)rhodium(I) (TRHHGB, 8). 8: chlorotris(triethylphosphine)platinum(II) tetrafluoroborate (TEPPTE, 3). 9: tris(triisopropylphosphine)hydridorhodium(I) (IPRHRH, 9). 10,11: (μ-carbonato)tris(triphenylphosphine)rhodium(I)bis(triphenylphosphine)rhodium(I)benzene solvate (CBTPRH, 10). 12, 15: chlorotris(triphenylphosphine)rhodium(I) (orange and red forms) (TPPRHC, 11, 12). 13: chlorotris(trimethylphosphine)rhodium(I) (TMPRHC, 13). 14: fluorotris(triethylphosphine)platinum(II) tetrafluoroborate (TEPPTB, 3). [b] For definition, see text. [c] Shortest C···C nonbonded contact between adjacent PR_3 groups. [d] Number of transformation matrix (see text) needed to generate the data points in cube 2 (compounds 1–4), cube 4 (compounds 5–12), cubes 1, 3, 5 (compounds 13–15). Translational components ($p2\pi/3$, $q2\pi/3$, $r2\pi/3$; p, q, r integer) are not given. For definition of cubes see Figure 6. [e] The first number refers to path 1, the second to path 2. See text.

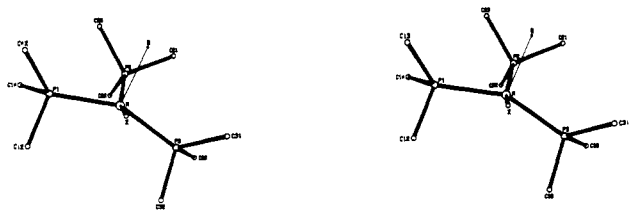

Figure 1. $XM(PC)_3$ skeleton showing atomic numbering. For conventions and definition of reference point Q see text (prepared with program ORTEP, ref 21).

2. Selection and Organization of Data

Atomic coordinates of 15 square-planar $XM(PR_3)_3$ molecules were retrieved from the CSD with programs provided by the Cambridge Crystallographic Data Center. The initial selection of structural fragments was effected through the CSD connectivity search program CONNS, consistency of atomic numering was achieved, and calculations of geometric parameters were performed with their program GEOM78.[20]

The following conventions were adopted (Figure 1): The three phosphorus atoms were designated P1, P2, and P3 with P2 trans to X. P1 was distinguished from P3 by requiring that the torsion angle P1–M–P2–P3 lay between −179.9 and 0.0°. A reference vector MQ was chosen to be approximately perpendicular to the mean XMP_3 plane[22] such that Q is on the same side of the plane as are X and P2. The conformational angles of the PR_3-group $P2R_3$ were measured with respect to Q and those of the PR_3-groups $P1R_3$ and $P3R_3$ with respect to P2. The carbon atoms were numbered such that their torsion angles ω_{2j}(C2j–P2–M–Q), ω_{1j}(C1j–P1–M–P2), and ω_{3j}(C3j–P3–M–P2) (j = 1, 2, 3) satisfy the condition $0 \le \omega_{i1} < \omega_{i2} < \omega_{i3} < 2\pi$($i$ = 1, 2, 3).

(19) Nie, N. H.; Hull, C. H.; Jenkins, J. G.; Steinbrenner, K.; Bent, D. H. "SPSS (Statistical Package for the Social Sciences)", 2nd ed.; McGraw-Hill: New York, 1975. Hull, C. H.; Nie, N. H.; "SPSS update 7-9"; McGraw-Hill, New York, 1981.

(20) For a description of general principles and methods of retrieving data from the CSD see: Murray-Rust, P.; Motherwell, S. *Acta Crystallogr., Sect. B* **1978**, *B34*, 2518.

(21) Johnson, C. K., ORTEP. Report ORNL-5138. Oak Ridge National Laboratory, Oak Ridge, Tennessee, **1976**.

(22) The hydrogen positional coordinates (X = H) are usually not available. We therefore approximated the best plane through atoms M, X, P1, P2, and P3 by the vector product (***MX1***) × (***MX2***), where (***MX1***) and (***MX2***) are defined as (***MX1***) = (***MP1***) + (***P1P2***)/2 and (***MX2***) = (***MP2***) + (***P2P3***)/2. This definition was used in all cases, even when the position of X was available. It is based on the assumption that the out of plane deformation angles $\delta(P_i) = \alpha(Q–M–P_i) - 90°$, etc., follow the condition $\delta(P1) = -\delta(P2) = \delta(P3) = -\delta(X)$. This is not an unreasonable assumption, since when coordinates of X *are* available (X ≠ H, 10 cases) $[\sum\{\delta(P1) + \delta(P2) + \delta(P3) + \delta(X)\}^2/4n]^{1/2} = 3.6°$.

The following structural parameters were calculated (Table I): the C*ij*–P*i*–M bond angles α_{ij}, the P1–M–P2 and P2–M–P3 bond angles α_{1M2} and α_{2M3}, respectively, the compound deviation $\delta = \{\delta(P1) - \delta(P2) + \delta(P3)\}/3$ of the Q–M–P angles from 90°, and the C2*j*–P2–M–Q, C1*j*–P1–M–P2 and C3*j*–P3–M–P2 torsion angles ω_{ij}. The quantity α_{ij} varies between 104 and 130°, α_{1M2} and α_{2M3} between 93 and 110°, and δ between 0 and 15°, ranges that are far larger than the uncertainty in any of the individual structure determinations.[23]

The torsion angles ω_{i1}, ω_{i2}, and ω_{i3} take values approximately but not exactly $2\pi/3$ apart (Table I). This is due to the fact that the PR_3 groups in the $XM(PR_3)_3$ molecule do not show exact threefold symmetry. A description of conformation in terms of these angles would depend on the particular choice of ω_{ij}. In order to eliminate such ambiguity a global conformational parameter ω_i is defined for each PR_3-group (Table I):

$$\omega_i = (\omega_{i1} + \omega_{i2} + \omega_{i3} - 2\pi)/3 \tag{1}$$

with

$$(\omega_{i1} < \omega_{i2} < \omega_{i3}) \tag{2}$$

For $0 \leq \omega_{i1} < \omega_{i2} < \omega_{i3} < 2\pi$ it follows that $0 \leq \omega_i \lesssim 2\pi/3$; if we define $2\pi/3 \leq \omega_{i1} < \omega_{i2} < \omega_{i3} < 8\pi/3$, it follows that $2\pi/3 \leq \omega_i \lesssim 4\pi/3$, etc.

3. Conformational Map

3.1. The Molecular Symmetry Group. A data base of 15 observed conformations may seem little, too little to allow conformational analysis of a system as complicated as $XM(PR_3)_3$. In order to make optimal use of the available information we must analyze the symmetry of the $XM(PC_3)_3$ fragment. Consider ω_1, ω_2, ω_3 as basis vectors spanning a three-dimensional conformational space that has the form of a cube with edges of lengths 2π. Each point in this cube corresponds to a molecular conformation. If we can obtain the symmetry of the conformational space, i.e., a representation of the molecular symmetry group in terms of the ω_i's, we can restrict our analysis to the asymmetric unit of the $(2\pi \times 2\pi \times 2\pi)$ cube. The symmetry group is required to include those operations on the ligand torsion angles that lead to images or mirror images of the initial conformation, i.e., to isometric structures.[18] Specifically, we require these operations to be internal rotations of the PR_3 groups around M–P bonds.[24]

In our case the PC_3 groups are considered as C_{3v}-symmetric rotors, the XMP_3 fragment as a C_{2v}-symmetric frame. We consider two types of operations. One is related to the number and nature of the rotors, the other is related to the nature of the frame to which these rotors are attached. Rotation of a set of three ligands C*ij* by $2\pi/3$ results in a cyclic permutation of the C*ij*'s. With the condition $\omega_{i1} < \omega_{i2} < \omega_{i3}$, this adds $2\pi/3$ to ω_i (eq 1 and 2). In general the result of rotating one or more PR_3 groups may be obtained with the help of transformation matrices $\boldsymbol{M}$

$$\omega' = \boldsymbol{M}\omega \tag{3}$$

$$\begin{bmatrix}\omega_1' \\ \omega_2' \\ \omega_3' \\ 1\end{bmatrix} = \begin{bmatrix}1 & 0 & 0 & p(2\pi/3) \\ 0 & 1 & 0 & q(2\pi/3) \\ 0 & 0 & 1 & r(2\pi/3) \\ 0 & 0 & 0 & 1\end{bmatrix}\begin{bmatrix}\omega_1 \\ \omega_2 \\ \omega_3 \\ 1\end{bmatrix} = \begin{bmatrix}\omega_1 + p(2\pi/3) \\ \omega_2 + q(2\pi/3) \\ \omega_3 + r(2\pi/3) \\ 1\end{bmatrix} \tag{4}$$

where $0 \leq p, q, r \leq 2$ with p, q, r integer. This implies that the $(2\pi \times 2\pi \times 2\pi)$ cube can be subdivided into 27 equivalent subcubes, each with edge $2\pi/3$, and it is sufficient to consider one subcube.

Rotation of the three PR_3 groups such that ω_1 changes to $-\omega_1$, ω_3 to $-\omega_3$, and ω_2 to $\pi - \omega_2$ corresponds to taking the mirror image of the starting conformation with respect to the XMP_3 plane while retaining the cyclic order in carbon atom numbering. The corresponding transformation matrix for the ω_i's is (5).

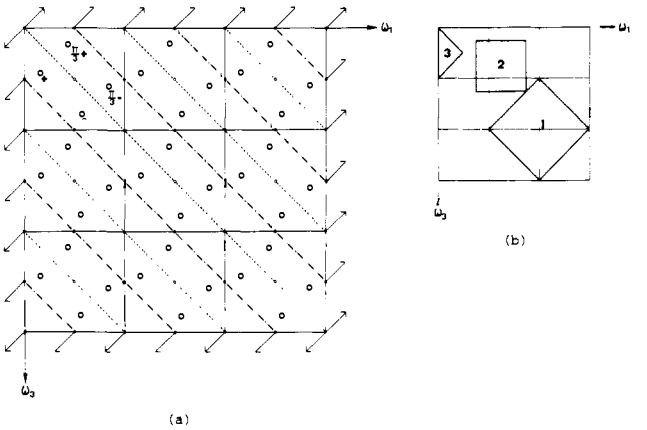

Figure 2. (a) Symmetry of conformational space projected down ω_2. Symbols: → twofold axes at $\omega_2 = 0, \pi/3$, etc.; ⇀ twofold screw axes at $\omega_2 = 0, \pi/3$, etc., with translation component $(\pi/3, 0, -\pi/3)$; - - - glide plane with translation component $(0, \pi/3, 0)$; ····· glide plane with translation component $(\pi/3, \pi/3, \pi/3)$; small circles, inversion centers at $\omega_2 = \pi/6, \pi/2$, etc.; large circles, a representative sample point at arbitrary coordinates $(\omega_1, \omega_2, \omega_3)$ and its symmetry-generated equivalents. (b) (1) the conventional unit cell given in ref 25 for space group $C2/c$ (origin in ω_2 at $\pi/6$); (2) unit cell of dimension $(2\pi/3 \times 2\pi/3 \times 2\pi/3)$ chosen for representation of data in Figures 3–6 (origin in ω_2 at 0); (3) asymmetric unit of conformational space $(0 \leq \omega_2 < 2\pi/3)$.

$$\begin{bmatrix}\bar{1} & 0 & 0 & 0 \\ 0 & \bar{1} & 0 & \pi \\ 0 & 0 & \bar{1} & 0 \\ 0 & 0 & 0 & 1\end{bmatrix} \tag{5}$$

$$\begin{bmatrix}0 & 0 & \bar{1} & 0 \\ 0 & \bar{1} & 0 & 0 \\ \bar{1} & 0 & 0 & 0 \\ 0 & 0 & 0 & 1\end{bmatrix} \tag{6}$$

$$\begin{bmatrix}0 & 0 & 1 & 0 \\ 0 & 1 & 0 & \pi \\ 1 & 0 & 0 & 0 \\ 0 & 0 & 0 & 1\end{bmatrix} \tag{7}$$

Similarly for the other mirror plane of the frame the matrix is given by (6) and for the twofold axis along XMP2 the matrix is given by (7). Each of the 27 subcubes now contains four equivalent points and can thus be subdivided into four elementary building blocks, called asymmetric units.

The order of the molecular symmetry group is $3 \cdot 3 \cdot 3 \cdot 4 = 108$. This means that we have $108 \cdot 15 = 1620$ points to sample the entire conformational space of $XM(PC_3)_3$, or, equivalently, that the 15 structures from the CSD can be concentrated into only $^1/_{108}$th of the full conformational space. Figure 2 shows a projection of the full conformational space down ω_2 with a representative sample point and its symmetry-equivalent points (conformational map). The picture may be considered as a finite part from an infinite three-dimensional lattice with unit cells of dimensions $(2\pi/3 \times 2\pi/3 \times 2\pi/3)$. The symmetries of infinite lattices in one, two, three, and four dimensions have all been derived, enumerated, tabulated exhaustively, and classified.[25] It would thus seem natural to use these same classifications also for conformational

(23) *R* factors of the crystal structure determinations are between 0.025 and 0.114 with $R < 0.05$ for 10 out of the 15 molecules.

(24) This is not the only possibility, but conceptually the simplest one. An alternative would be to admit breaking M–P bonds and re-forming them in new conformations.

(25) "International Tables for X-Ray Crystallography"; Kynoch Press: Birmingham, England, 1969; Vol. I. Brown, H.; Bülow, R.; Neubüser, J.; Wondratschek, H.; Zassenhaus, H., "Crystallographic Groups of Four-Dimensional Space", Wiley-Interscience, New York, 1978.

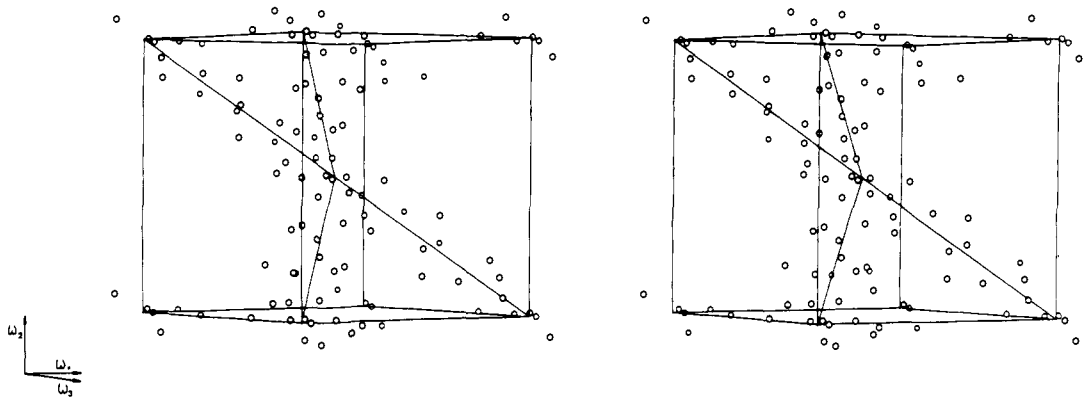

Figure 3. Distribution of data points in conformational space (conformational map) in the range $5\pi/12 \leq \omega_1 \leq 15\pi/12$, $-\pi/12 \leq \omega_2 \leq 9\pi/12$, $\pi/12 \leq \omega_3 \leq 11\pi/12$. The cube shown corresponds to unit cell 2 in Figure 2b; the body diagonals are discussed in the text (prepared with program ORTEP, ref 21).

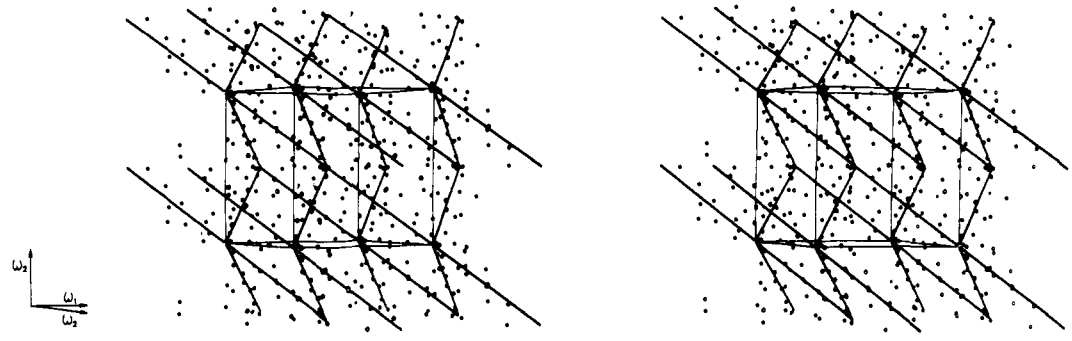

Figure 4. Conformational map enclosing a volume of (2 × 2 × 2) units cells. The cube shown corresponds to unit cell 2 in Figure 2b. Linear paths 1 and zig-zag paths 2 are shown by thick lines (prepared with program ORTEP, ref 21).

maps,[15,26,27] supplemented only by specification of the cyclic boundary conditions

$$\omega' = M\omega(\text{mod } 2\pi) \tag{3a}$$

The particular example of Figure 2 shows a projection of the symmetry of a three-dimensional lattice called $C2/c$ in International Tables for X-ray Crystallography.[25] The symbol C expresses translational symmetry (matrix 4), 2 expresses the twofold rotational symmetry of conformational space (matrix 6), and c expresses a combined translation–mirror symmetry (glide plane, matrix 7).[28] An inversion operation (matrix 5) is not contained in the space group symbol because it follows from 2 and c.

Each point in conformational space corresponds to a particular molecular conformation. In particular, a point that lies on a symmetry element of conformational space and is consequently transformed into itself by the corresponding symmetry operation maps a molecular conformation that is transformed into itself by an element of molecular covering symmetry. Thus, points coinciding with inversion centers in conformational space correspond to molecular conformations exhibiting mirror symmetry with respect to the plane XMP_3. Points coinciding with twofold axes in conformational space correspond to molecular conformations that are mirror-symmetric with respect to the plane containing X, Q, and P2.

In this section, it was shown that analysis of the molecular symmetry group of a nonrigid model of the $XM(PR_3)_3$ molecule reduces the volume of conformational space to be analyzed. The reduction factor equals the order of the molecular symmetry group, 108 in the present case. The symmetry of conformational space can be classified on the basis of crystallographic space group symmetry. Finally, each point in conformational space is associated with a molecular conformation, special positions being associated with symmetric molecular conformations.

3.2. Conformational Map of $XM(PR_3)_3$, Scattergrams. Taking into account the symmetry discussed in the previous section the 15 data points were expanded into a set that covers a volume somewhat larger than one unit cell. The distribution of these points, the conformational map of the $XM(PC_3)_3$ fragment, is shown as a stereo diagram in Figure 3. Inspection shows that the points are not at all randomly distributed in the unit cell cube but are concentrated in the neighborhood of body diagonals (indicated as solid lines in Figure 3). Other regions of the cube are conspicuously empty.[29] We conclude that $XM(PR_3)_3$ molecules show certain preferred conformations.

The populated areas in Figure 3 are continuous, not discrete. One such area is along the body diagonal between $(\omega_1, \omega_2, \omega_3) = (\pi/2, 2\pi/3, \pi/6)$ and $(7\pi/6, 0, 5\pi/6)$ (see Figure 2). This area—we call it path 1—continues as the body diagonal of neighboring unit cells (Figure 4). Two other continuously populated areas extend from $(\pi/2, 2\pi/3, 5\pi/6)$ to $(5\pi/6, \pi/3, \pi/2)$ and on to $(\pi/2, 0, 5\pi/6)$. They make up path 2, which takes a zig-zag course through conformational space, thereby interconnecting parallel paths 1 in neighboring unit cells. Because of symmetry the asymmetric unit of path 1 is a quarter of the body diagonal, e.g., the straight line between the corner at $(\pi/2, 2\pi/3, \pi/6)$ and the inversion center at $(2\pi/3, \pi/2, 2\pi/3)$. The asymmetric unit for path 2 is defined similarly.

We conclude that preferred conformations change continuously along discernible pathways; changes in ω_1, ω_2 and ω_3 are simultaneous and correlated. The significance of these correlations is analyzed in Figure 5. It shows the panorama of PC_3 confor-

(26) Murray-Rust, P.; Bürgi, H. B.; Dunitz, J. D. *Acta Crystallogr., Sect. A* **1979**, *A35*, 703.
(27) Bürgi, H. B. *Match* **1980**, *9*, 13.
(28) The conventions adopted by "International Tables for X-Ray Crystallography" require unit cell edges in the family of monoclinic lattices to be parallel to an axis or plane of symmetry and their origins to coincide with centers of symmetry if any. In order to demonstrate the correspondence between matrices 4–7 and space group $C2/c$ a transformation of base vectors is necessary: $\mathbf{a} = \omega_1 + \omega_3$, $\mathbf{b} = \omega_1 - \omega_3$, $\mathbf{c} = \omega_2$, shift of origin along ω_2 by $\pi/6$. Unit cell constants are $a = b = 2^{1/2}2\pi/3$, $c = 2\pi/3$. Matrices 4–7 have to be transformed accordingly.
(29) If this was not noticed before, it is probably because the available data points appear to be scattered all over the $(2\pi \times 2\pi \times 2\pi)$ cube of conformational space and only a symmetry analysis reveals the underlying pattern.

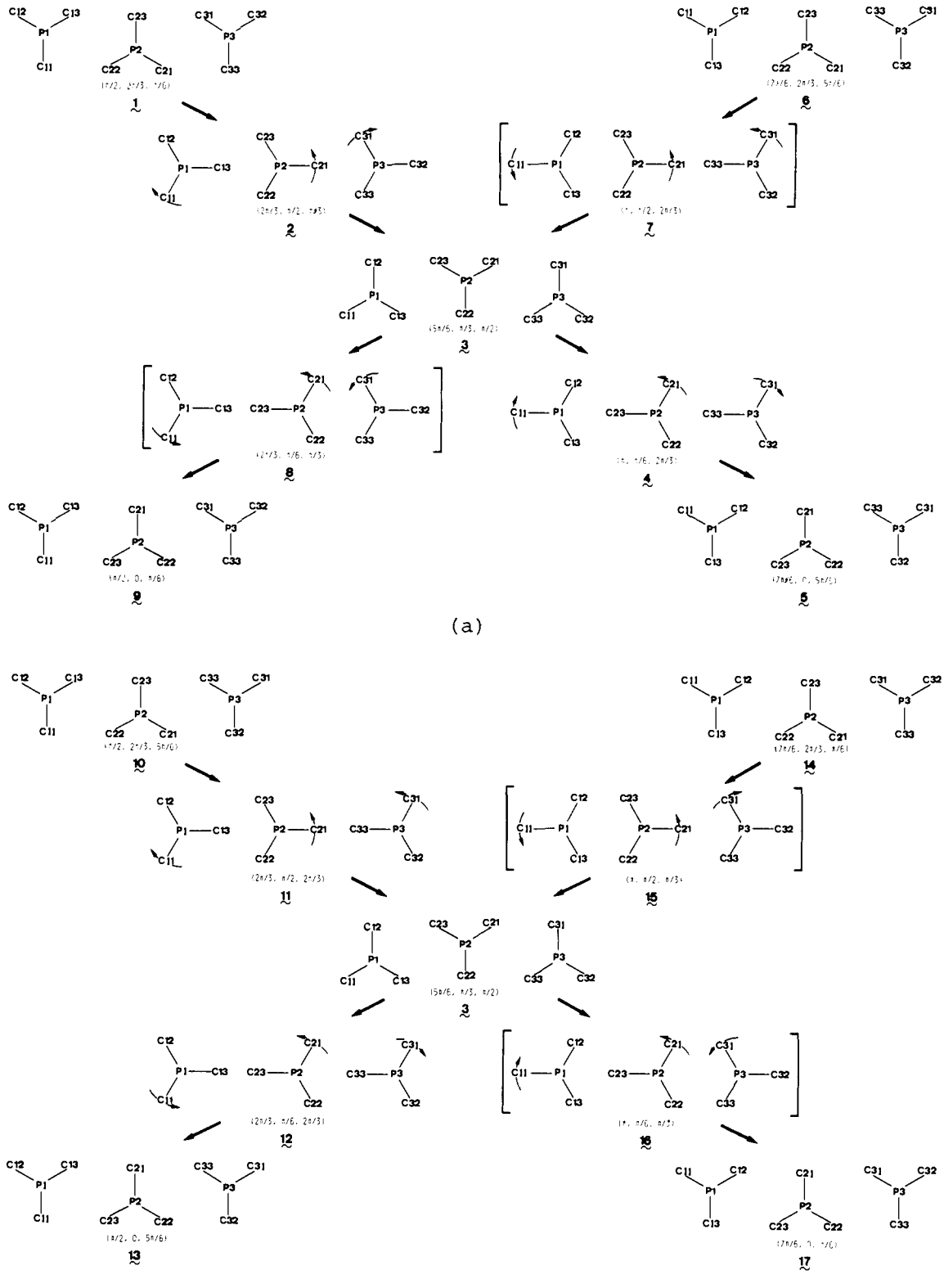

Figure 5. Schematic representation of $XM(PC_3)_3$ conformations: the panorama of PC_3 groups as seen by an observer at M. Note the one to one correspondence between conformations 1–17 and the points in conformational space given in brackets. (a) Conformations **1–5** illustrate the gearing of PC_3 groups along path 1. (b) Conformations **10**, 11, **3**, **12**, **13** illustrate the combination of gearing and gear clashing in path 2.

mations as seen by an observer sitting at M (cylindrical projection). Each projection corresponds to a point on one of the four body diagonals in conformational space. The points corresponding to successive projections are a quarter of a body diagonal apart (Figure 3).

Along path 1 (Figure 5a, **1** → **2** → **3** → **4** → **5**) the carbon substituents on the phosphorus atoms avoid each other as well as they can to achieve optimal packing of the carbon protuberences of one PR_3 ligand into the hollows of adjacent PR_3 ligands. In order to maintain this mode of packing along the entire path any change in conformation of one PR_3 group necessitates conformational changes of the others in a manner that is reminiscent of meshed cogwheels undergoing a gearing motion. If $P1R_3$ rotates in a clockwise direction, $P2R_3$ rotates in counterclockwise and $P3R_3$ in a clockwise direction. It seems reasonable to attribute the coupling to nonbonded interactions between the tightly in-

Table II. Results of Regression Analyses on Scattergrams of α vs. ω (Figure 7)[a]

path	group	R	α_0, deg	α_1, deg	α_2, deg	α_4, deg	R_1^2	R_2^2	R_4^2	no. of cases
1	P1, P3	all	115.7	6.4 (4)		2.3 (4)	0.665		0.755	84
	P1, P3	alkyl	115.2	6.2 (5)	1.0 (5)		0.787	0.809		36
	P1, P3	Ph	116.1	6.0 (5)		4.1 (6)	0.618		0.824	48
2	P1, P3	all	116.3	7.3 (5)		1.7 (5)	0.750		0.770	132
	P1, P3	alkyl	115.8	7.2 (4)	2.7 (4)		0.826	0.884		84
	P1, P3	Ph	117.1	4.9 (12)		5.0 (13)	0.646		0.735	48
1	P2	all	116.2	0.0		4.9 (4)			0.644	84
	P2	alkyl	116.2	0.0		3.3 (5)			0.615	36
	P2	Ph	116.4	0.0	−1.4 (7)	6.7 (6)		0.026	0.736	48
2	P2	all	115.7	0.0		4.6 (3)			0.672	132
	P2	alkyl	115.5	0.0	−1.0 (4)	3.5 (4)		0.032	0.642	72
	P2	Ph	116.2	0.0	−1.6 (6)	6.2 (5)		0.029	0.775	60

[a] $\alpha = \alpha_0 + \alpha_1 \cos\omega + \alpha_2 \cos 2\omega + \alpha_4 \cos 4\omega$ (ref 32 and 33); R_i^2 are the corresponding correlation coefficients taking into account terms up to and including α_i.

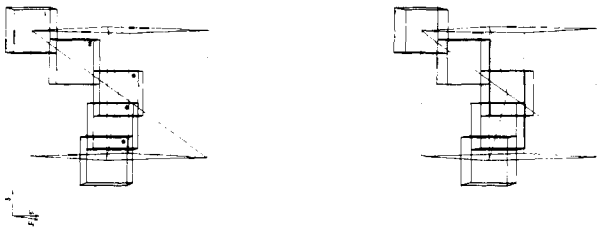

Figure 6. Allocation of data to the two paths. Path 1 comprises data points in cubes 1–3, path 2 comprises those in cubes 3–5 (prepared with program ORTEP, ref 21).

termeshed PR_3 groups. Along the second diagonal in Figure 5a (**6** → **7** → **3** → **8** → **9**) the directions of rotation of $P1R_3$ and $P3R_3$ are reversed and all three PR_3 groups rotate in the same sense. As a consequence, ligands of neighboring PR_3 groups oppose each other as in **7** and **8**. On the basis of the nonbonded interaction involved, such conformations would seem to be energetically unfavorable, and indeed, such conformations are not observed experimentally: the corresponding part of conformational space is empty (Figure 3). Note that the unfavorable conformation **7**, for example, shows one very close approach of C21 and C33 in the XMP_3 plane as well as two close approaches of C12 to C23 and C13 to C22 disposed symmetrically with respect to the XMP_3 plane. The two partial conformations are structurally and energetically inequivalent. Their relative stability can be gauged by analyzing path 2.

Figure 5b shows the cylindrical projections for conformations corresponding to the remaining two body diagonals of the cube in Figure 4. The starting conformation **10** of path 2 (**10** → **11** → **3** → **12** → **13**) is the same as **1** in path 1 except for $P3R_3$ which has been rotated by $2\pi/3$. In path 2 rotation of $P2R_3$ and $P3R_3$ is in the same, counterclockwise direction leading to conformation **11** with C21 and C33 opposing each other in the XMP_3 plane. Continuation along this direction leads to **3**, a mirror image of **10**, and then to **16** in which C21 and C31 as well as C22 and C33 oppose each other. The latter conformation is not observed, however: the corresponding part of conformational space is empty. Instead, the path bends back by reversing the direction of rotation of $P1R_3$ and $P3R_3$ and leads to **12**, which is mirror symmetric to **11**. Along this path $P1R_3$ behaves like a meshed gear in the first half, like an opposing gear in the second half, and vice versa for $P3R_3$. From these results we have to conclude that the partial conformation with two atoms opposing each other as in **11** and **12** is energetically more favorable than the opposing arrangement of four atoms as in **15** and **16**.

So far we have restricted our discussion to conformation. In the following paragraphs we shall analyze the consequences of continuous conformational changes on other structural parameters listed in Table I.

4. Detailed Reaction Paths for Conformational Interconversions

4.1. Symmetry Aspects. In section 3.1 a representation of the molecular symmetry group in terms of the ω_i's was given. An extension of the analysis to nine ω_{ij}'s, nine α_{ij}'s, two α_{iMj}'s, and one δ requires an extended representation of the group in terms of all 21 structural parameters. Transformation matrices analogous to matrices 4–7 may be written in terms of individual blocks of the following dimensions: (7 × 7) for the ω_{1j}'s and ω_{3j}'s, (4 × 4) for the ω_{2j}'s, (6 × 6) for the α_{1j}'s and α_{3j}'s, (3 × 3) for the α_{2j}'s, (2 × 2) for α_{1M2} and α_{2M3}, (1 × 1) for δ. The blocks are given in the same sequence as for the ω_i's. The following matrices operate on the column vector (ω_{11}, ω_{12}, ω_{13}, ω_{31}, ω_{32}, ω_{33}, 1):

$$\left[\begin{array}{ccc|ccc|c} 1&0&0&0&0&0&0\\ 0&1&0&0&0&0&0\\ 0&0&1&0&0&0&0\\ \hline 0&0&0&1&0&0&0\\ 0&0&0&0&1&0&0\\ 0&0&0&0&0&1&0\\ \hline 0&0&0&0&0&0&1 \end{array}\right] \quad (4a)$$

$$\left[\begin{array}{ccc|ccc|c} \bar{1}&0&0&0&0&0&0\\ 0&0&\bar{1}&0&0&0&0\\ 0&\bar{1}&0&0&0&0&0\\ \hline 0&0&0&\bar{1}&0&0&0\\ 0&0&0&0&0&\bar{1}&0\\ 0&0&0&0&\bar{1}&0&0\\ \hline 0&0&0&0&0&0&1 \end{array}\right] \quad (5a)$$

$$\left[\begin{array}{ccc|ccc|c} 0&0&0&\bar{1}&0&0&0\\ 0&0&0&0&0&\bar{1}&0\\ 0&0&0&0&\bar{1}&0&0\\ \hline \bar{1}&0&0&0&0&0&0\\ 0&0&\bar{1}&0&0&0&0\\ 0&\bar{1}&0&0&0&0&0\\ \hline 0&0&0&0&0&0&1 \end{array}\right] \quad (6a)$$

$$\left[\begin{array}{ccc|ccc|c} 0&0&0&1&0&0&0\\ 0&0&0&0&1&0&0\\ 0&0&0&0&0&1&0\\ \hline 1&0&0&0&0&0&0\\ 0&1&0&0&0&0&0\\ 0&0&1&0&0&0&0\\ \hline 0&0&0&0&0&0&1 \end{array}\right] \quad (7a)$$

The matrices 4b–7b operate on the column vector (ω_{21}, ω_{22}, ω_{23}, 1):

$$\left[\begin{array}{ccc|c} 1 & 0 & 0 & 0 \\ 0 & 1 & 0 & 0 \\ 0 & 0 & 1 & 0 \\ \hline 0 & 0 & 0 & 1 \end{array}\right] \quad (4b)$$

$$\left[\begin{array}{ccc|c} \bar{1} & 0 & 0 & \pi \\ 0 & 0 & \bar{1} & \pi \\ 0 & \bar{1} & 0 & \pi \\ \hline 0 & 0 & 0 & 1 \end{array}\right] \quad (5b)$$

$$\left[\begin{array}{ccc|c} \bar{1} & 0 & 0 & 0 \\ 0 & 0 & \bar{1} & 0 \\ 0 & \bar{1} & 0 & 0 \\ \hline 0 & 0 & 0 & 1 \end{array}\right] \quad (6b)$$

$$\left[\begin{array}{ccc|c} 1 & 0 & 0 & \pi \\ 0 & 1 & 0 & \pi \\ 0 & 0 & 1 & \pi \\ \hline 0 & 0 & 0 & 1 \end{array}\right] \quad (7b)$$

Matrices 4a–7b account for symmetry operations related to the C_{2v}-symmetric frame XMP_3, but not for rotation of an individual PR_3 group. These are obtained easily by replacing the appropriate (3 × 3) block in (4a) or (4b) by either

$$\begin{bmatrix} 0 & 1 & 0 \\ 0 & 0 & 1 \\ 1 & 0 & 0 \end{bmatrix} \text{ or } \begin{bmatrix} 0 & 0 & 1 \\ 1 & 0 & 0 \\ 0 & 1 & 0 \end{bmatrix} \quad (8)$$

to obtain cyclic permutations of the corresponding atoms C*ij*. All transformations are subject to the side condition $0 \leq \omega_{i1} < 2\pi$ and $\omega_{i1} < \omega_{i2} < \omega_{i3}$ (eq 2).

The (6 × 6) matrices 4c–7c and the (3 × 3) matrices 4d–7d operating on (α_{11}, α_{12}, α_{13}, α_{31}, α_{32}, α_{33}) and (α_{21}, α_{22}, α_{23}) are obtained from matrices 4a–7b by deleting the last row and the last column and changing $\bar{1}$ into 1. Modifications of (4c) and (4d) to account for rotation of a single PR_3 group are the same as for (4a) and (4b). The (2 × 2) matrices operating on (α_{1M2}, α_{2M3}) and (1 × 1) matrices operating on δ are

$$\begin{bmatrix} 1 & 0 \\ 0 & 1 \end{bmatrix} \quad \begin{bmatrix} 0 & 1 \\ 1 & 0 \end{bmatrix} \quad [1] \quad [\bar{1}]$$

(4e,5e) (6e,7e) (4f,5f) (6f,7f)

With these transformations it is possible to generate data vectors with 21 components, one for each of the symmetry-equivalent conformations in Figure 2.

4.2. Data Organization. All further analyses have been done for path 1 and path 2 separately. It was therefore necessary to assign the data points as belonging to one, the other, or both. We have defined equal cubes of dimension $(2^{1/2}\pi/6)^3$ enveloping all data points. Figure 6 shows three cubes, 1, 2, and 3, along the body diagonal of path 1 and three cubes, 3, 4, and 5, along the body diagonal of path 2. The body centers of cubes 1, 2, and 3 refer to conformations **1**, **2**, and **3** (Figure 5a), those of 3, 4, and 5 refer to conformations **3**, **12**, and **13** (Figure 5b). Cubes 1 and 3 are related by a center of inversion at $(2\pi/3, \pi/2, \pi/3)$ and cubes 3 and 5 by one at $(2\pi/3, \pi/6, 2\pi/3)$. Cube 3 at the center of the unit cell contains a twofold axis perpendicular to and through the center of its face next to the observer. This twofold axis generates a further cube 2′ (not shown) from 2 to complete the full length of path 1. The full length of path 2 including cube 4′ is generated likewise.[30] Path 1 has 6 points (3 symmetry independent ones) each in cubes 1 and 3 and 8 (4) each in cubes 2 and 2′. Path 2 has 6 (3) points each in cubes 5 and 3 and 16 (8) each in cubes 4 and 4′. When the transformations from Section 4.1 are used, a set of 28 data vectors is generated for path 1 and a set of 44 vectors for path 2, each of them with 21 components. Subsequent analyses have been done with some or all of these components.

4.3. Dependence of Bond Angles α_{ij} on Torsion Angles ω_{ij}. As mentioned in the introduction the C–P–M bond angles cover a range of about 25°. We have analyzed this variation by plotting the angles α_{1i} and α_{3i} vs. ω_{1i} and ω_{3i} (for path 1 see Figure 7a) and α_{2i} vs. ω_{2i} (for path 1 see Figure 7d).[31] Scattergram 7a shows a sinusoidal dependence of α on ω. There is a maximum (and a symmetry point) at $\omega = 0$ that reflects the situation of C13 in conformation **2** (Figure 5). There is a minimum (and another symmetry point) at $\omega = \pi$ that reflects the situation of C32 in conformation **2**. Thus α tends to be large when a substituent R of $P1R_3$ or $P3R_3$ points toward $P2R_3$ and small if it points toward the sterically less demanding X.

Deviations from sinusoidal behavior are also seen in Figure 7a, especially in the neighborhood of $\omega = \pi/2$. Our suspicion that bulges in the scattergram were due to triphenylphosphine ligands was confirmed by separate scattergrams for the two families of compounds with R = alkyl and R = Ph, respectively (Figure 7b,c). Figure 7c indicates a modulation on top of the sinusoidal behavior, which is not present in Figure 7b. Analogous diagrams for path 2 are not shown but look very similar. Figure 7d shows the scattergram for α_{2i} vs. ω_{2i}. It has two pairs of symmetry-equivalent maxima and symmetry points at 0 and π and at $\pi/2$ and $3\pi/2$, respectively, with minima in-between. The first pair of maxima reflects situations like that of C23 in conformation **1**, the second pair reflects situations like that of C21 in conformation **2**.

To gain a more quantitative picture of these correlations the data for $P1R_3$ and $P3R_3$ have been fitted to the following expression:

$$\alpha = \alpha_0 + \alpha_1 \cos \omega + \alpha_2 \cos 2\omega + \alpha_4 \cos 4\omega \quad (9)$$

Table II shows the coefficients α_0, α_1, α_2, α_4, and the corresponding correlation coefficients. Results are given only when judged significant on the basis of a statistical *F*-test.[32] For $P1R_3$ and $P3R_3$ the mean CPM angle α_0 is about 116°, for both paths. The amplitude α_1 is ~6° and accounts for about 60 to 80% of the variance in α. The contributions of α_2 and α_4 are different in the two paths but may absorb another 2 to 20% of the total variance. There are hardly any significant differences between path 1 and path 2.

The data for $P2R_3$ (Figure 7d) have been fitted to

$$\alpha = \alpha_0 + \alpha_2 \cos 2\omega + \alpha_4 \cos 4\omega \quad (10)$$

The coefficients are listed in Table II.[33] The mean angle α_0 is about 116° as before, α_2 seems to be relatively unimportant, α_4 expresses the dominant feature in Figure 7d and is significant for all cases. For $P2R_3$, eq 10 accounts for about 60 to 75% of the

(30) The twofold axis also generates cubes 1′ and 5′ from 1 and 5 corresponding to conformations **5** (Figure 5a) and **10** (Figure 5b), respectively. However, cube 1′ is equivalent to cube 1 by translation $(2\pi/3, -2\pi/3, 2\pi/3)$ along $(\omega_1, \omega_2, \omega_3)$, so that cubes 1, 2, 3, and 2′ encompass the full data set of path 1 within one unit cell; similarly for path 2 the full data set would comprise the points in cubes 5, 4, 3, and 4′.

(31) Many of the correlations discussed in this paper have been discovered only after performing extensive factor analyses (ref 19). Once discovered, the correlations are interpreted in stereochemical terms. It is this latter step, also called reification, which we discuss here. The details of factor analyses are not reported because they do not by themselves add insight into the conformational behavior of the compounds investigated. For details of the procedure see: Murrary-Rust, P.; Motherwell, S.; *Acta Crystallogr., Sect. B* **1978**, *B34*, 2534.

(32) Terms in α_3 and α_6 were statistically insignificant in all cases investigated here. Terms in α_5, α_7, were very small, but sometimes statistically significant. They did not add qualitatively new aspects to the interpretation of the correlations and are not reported here.

(33) Terms in α_1 are exactly zero, because the periodicity in ω of these scattergrams is π rather than 2π (Figure 7d).

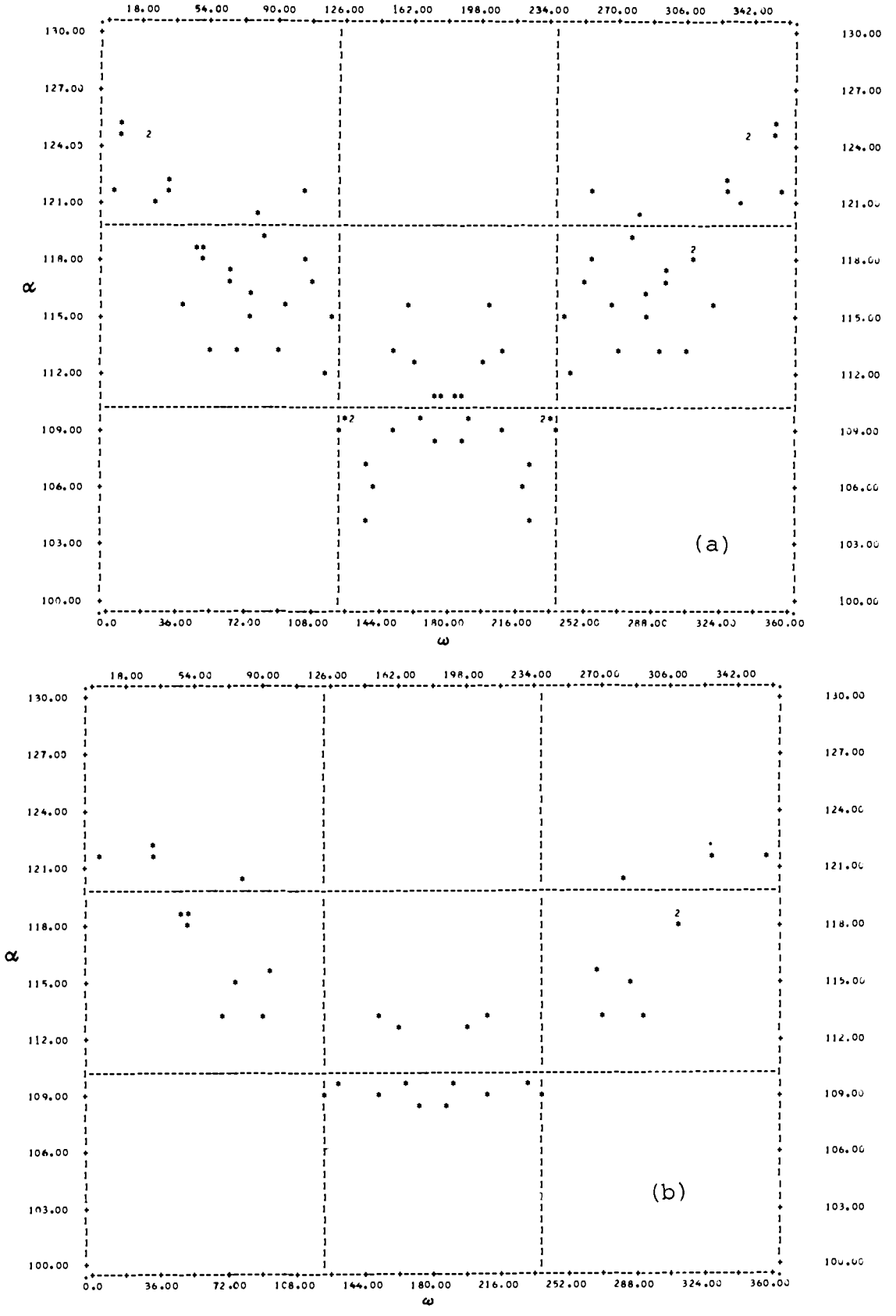

Figure 7. Scattergrams of ω_{ij} vs. α_{ij} for path 1. (a) All data, (b) R = alkyl, (c) R = Ph, for rotors $P1R_3$ and $P3R_3$ and (d) all data for rotor $P2R_3$

total variance in observed angles.

4.4. Structural Interpretation of Empirical Correlations. Having shown a systematic dependence of bond angles α_{ij} on conformational angles ω_{ij} we now try to give a geometric interpretation of eq 9 and 10. We consider the PR_3 groups as C_{3v}-symmetric rotors attached to the C_{2v}-symmetric XMP_3 frame. Since an arbitrary

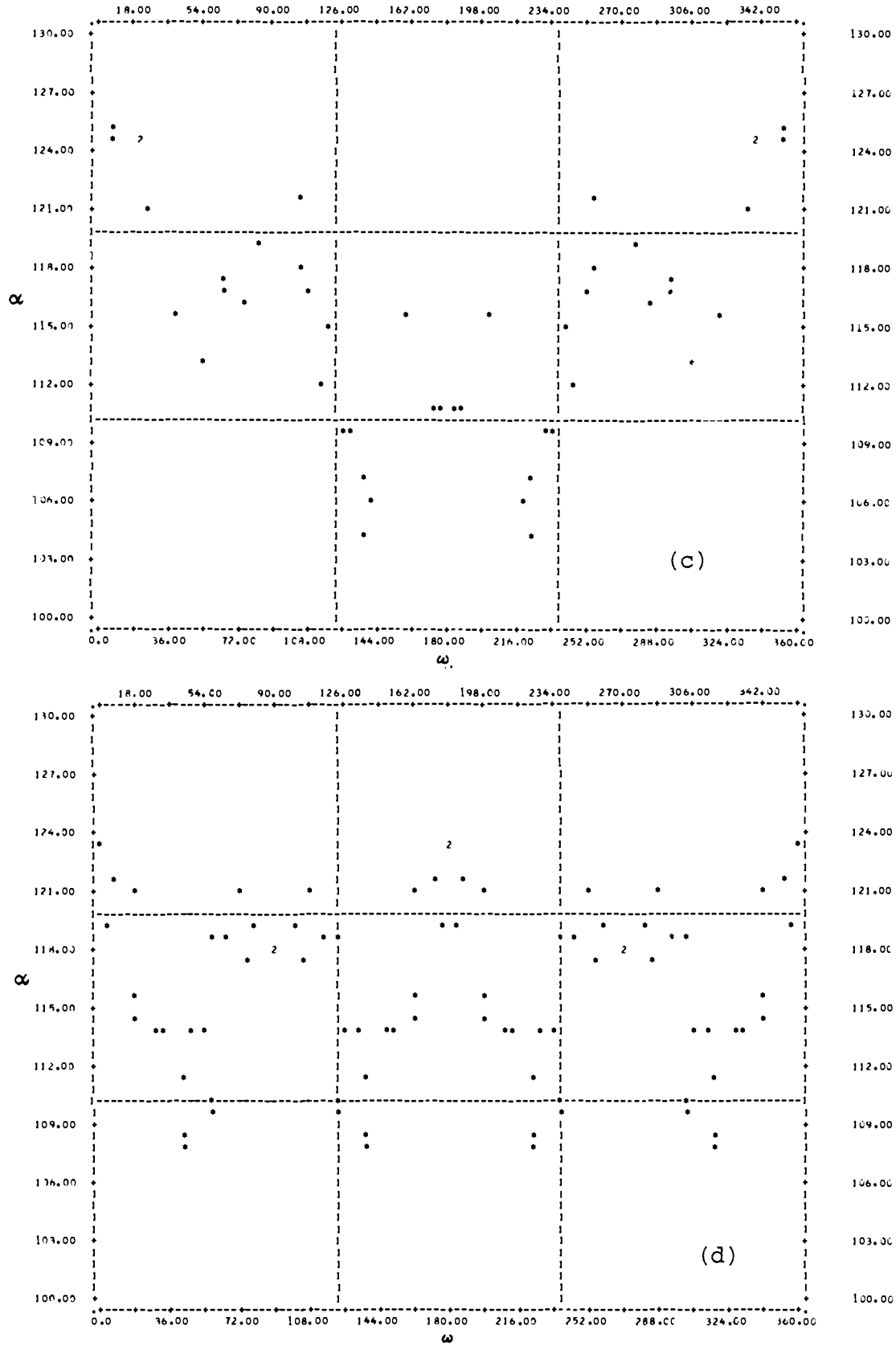

(prepared with program SPSS, ref 19).

conformation (ω_1, ω_2, ω_3) of the $XM(PR_3)_3$ molecules has no covering symmetry, there is in general no reason for the local C_3 axis of the PR_3 groups to coincide with the corresponding M–P bond direction. A general geometrical model for such deviations and its structural consequences are elaborated in the Appendix. The main points are summarized below.

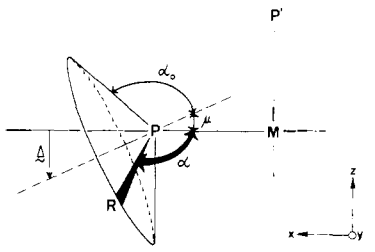

Figure 8. Geometrical model used to analyze deviations of the local threefold axes of PR3 from the direction of the M–P bond.

We define a local coordinate system for each PR_3 rotor as in Figure 8. For $P1R_3$ and $P3R_3$, a displacement vector Δ of the C_3 axis from the M–P bond direction may be given as a function of conformation by the expression (see Appendix, supplementary material)

$$\Delta = (0, \sum_{n=1}^{N} \Delta_{3n}{}^{y} \sin 3n\omega, \sum_{n=0}^{N} \Delta_{3n}{}^{z} \cos 3n\omega) \qquad (11)$$

where $\Delta_{3n}{}^{y}$ and $\Delta_{3n}{}^{z}$ are displacement vector components along the y and z axes, respectively. The angular displacement vector Δ is a function of ω and has to conform to the overall symmetry of the nonrigid molecule. Specifically, it has to be unchanged when the PR_3 group is rotated by $2\pi/3$. Another condition is that symmetry operations like 4–7 must lead to isometric structures. These conditions are incorporated in eq 11, which describes the group $P1R_3$. A similar equation holds for $P2R_3$,

$$\Delta = (0, \sum_{n=1}^{N} \Delta_{3n}{}^{y} \cos 3n\omega, \sum_{n=1}^{N} \Delta_{3n}{}^{z} \sin 3n\omega) \qquad (12)$$

The effect of these displacements on the positions of the ligand Cij and on the corresponding bond angles α_{ij} are obtained via a geometric argument given in the appendix.

With $N = 1$ the result is, for $P1R_3$,

$$\begin{aligned} \alpha &= \alpha_0 - \Delta_0{}^{z} \cos \omega + \Delta_1{}^{y} \sin \omega \sin 3\omega - \Delta_1{}^{z} \cos \omega \cos 3\omega \\ &= \alpha_0 + \alpha_1 \cos \omega + \alpha_2 \cos 2\omega + \alpha_4 \cos 4\omega \end{aligned} \qquad (13)$$

Similarly for $P2R_3$

$$\begin{aligned} \alpha &= \alpha_0 - (\Delta_1{}^{y} \sin \omega \sin 3\omega + \Delta_1{}^{z} \cos \omega \cos 3\,\omega) \\ &= \alpha_0 + \alpha_2 \cos 2\omega + \alpha_4 \cos 4\omega \end{aligned} \qquad (14)$$

Note that eq 13 and 14 are of the same form as eq 9 and 10. Whereas the former are the result of a geometric argument, independent of the experimental data, the latter are needed to fit the observed distributions of α vs. ω. Thus the observed dependence of α_{ij} on ω_{ij} can be interpreted in terms of a PR_3 group whose local approximate threefold axis is not collinear with the adjacent M–P bond and may even change orientation as a function of ω: the term in α_1 ($=-\Delta_0{}^{z}$, eq 11) indicates a misalignment of the local threefold axis of $P1R_3$ independent of conformation. The numerical data (Table II) together with Figure 8 show that this distortion helps to increase the separation to $P2R_3$. For reasons of symmetry such a distortion is impossible for $P2R_3$ (see Appendix and footnote 33). The terms in α_2 and α_4 represent precession motion of the local threefold axes, synchronized with changes in ω; the precession frequency is 3ω.[34] Because $\alpha_2 \sim 0$, $\Delta_3{}^{y} \sim \Delta_3{}^{z} \sim -\alpha_4$ and the path traced by the precessing local threefold axis is approximately circular. Analysis of the numerical data in Table II shows that the conformation-dependent parts of the distortion (α_2, α_4) also serve to increase the distance between neighboring PR_3 groups and thereby to minimize nonbonded interactions. This is especially clear for conformations such as **1**, **3**, etc., in which the local threefold axes of $P1R_3$, $P2R_3$, and $P3R_3$ are displaced out of the mean plane of the XMP_3 fragment, alternatingly up and down (eq 11 and 12). As will be shown below this distortion accentuates an analogous distortion in the same direction of the M–P bonds themselves out of the mean plane of the XMP_3 fragment.

The above analysis treats the dependence of bond angle on conformational angle for each phosphine ligand separately. It does not take into account the two types of coupling of PR_3 conformations described in the previous sections. A more detailed analysis did not seem justified, however, since the database was too meager for meaningful results.

Deviations of local threefold axes from Rh–P bond directions have been described for $HRh(P\{CH(CH_3)_2\}_3)_3$ and interpreted in terms of bent Rh–P bonds due to overcrowding between cis positioned phosphine ligands.[9] A similar geometrical model has been used[35] to describe the inequality of H–C–X bond angles in CH_3OH, CH_3SH, CH_3OCH_3, CH_3SCH_3, CH_3NH_2, CH_3NHCH_3, or C–Y–X angles in $(CH_3)_3CCH_2C(CH_3)_3$, $HX(Y(CH_3)_3)_3$ (X, Y = C, Si). In all of these molecules the CH_3 or $Y(CH_3)_3$ group is in an environment of lower than C_{3v} symmetry. The tilt angles α_1 are between 2 and 4°. The model on which eq 11 and 12 are based is more general; it can be applied to any rotor in any conformation and of any multiplicity, attached to special or general positions of frames of any symmetry. Furthermore, it allows to describe misalignment of the rotor with respect to the adjacent bond independently of conformation, as well as reorientation of the rotor coupled to conformational changes.

We are not aware of any spectroscopic observations of dynamic displacements of local symmetry axes, but to the extent that the correlations between structural parameters are models of conformational interconversion pathways (see discussion) these displacements have to occur in dynamic systems as well.

5. Further Correlations Between Conformation and Other Geometrical Parameters

So far it has been shown that changes in conformation of the three PR_3 groups are strongly coupled to each other and to changes in C–P–M bond angles. Analysis of other parameters, e.g., the nonplanarity parameter δ and the P–M–P bond angles, has been performed as follows: For each of the two pathways the corresponding data points (ω_1, ω_2, ω_3) were projected onto the appropriate body diagonal (Figure 3) and normalized to yield values of p between 0 and 1. Thus conformations **1**, **2**, **3**, **4**, **5** have p values of 0, 0.25, 0.5, 0.75, and 1, respectively. Figure 9 shows scatterplots of δ vs. p; they are periodic in p with period unity. For path 1 (Figure 9a) it is seen that at $p = 0$, i.e., for conformation **1**, the noncoplanarity of P1, P2, P3, and M is an extremum, for **2** ($p = 0.25$) it has to be zero because this conformation is mirrorsymmetric with respect to the XMP_3 plane, and for **3** ($p = 0.5$) the nonplanarity has the same magnitude as for **1** but the opposite sign. Of the total variance in Figure 9a, 85% may be explained by a relationship of the form

$$\delta = -8.2\ (7)^\circ \cos 2\pi p \qquad (15)$$

For path 2 extreme nonplanarity is found at $p \sim 0.1$ and 0.4, i.e., between conformations **10** and **11**, and **11** and **3**, respectively. A correlation coefficient (r^2) of 0.73 is obtained for the relationship

$$\delta = -8.0\ (1.2)^\circ \cos 2\pi p - 4.1\ (1.3)^\circ \sin 4\pi p$$

This function has extrema at $p = 0.08$ and 0.42 with $|\delta| = 10.5°$.[36] These values show that the increase of steric interaction between atoms C21 and C33 consequent to the transition from conformation **10** to **11** is initially made as small as possible by an accompanying out of plane deformation. Note that for $0.6 \lesssim p \lesssim 0.9$ the scatterplot Figure 9b is empty, demonstrating that

(34) This is perhaps not obvious, but is straightforward. It takes a lot of space to explain, and we leave the problem for the reader's entertainment. (How do α_2 and α_4 determine the sense of the precession motion?)

(35) See, for example: Flood, E.; Pulay, P.; Boggs, J. E. *J. Am. Chem. Soc.* **1977**, *99*, 5570. Pross, A.; Radom, L.; Riggs, N. V. *Ibid.* **1980**, *102*, 2253. Bartell, L. S.; Bradford, W. F. *J. Mol. Struct.* **1977**, *37*, 113. Doun, S. K.; Bartell, L. S. *Ibid.* **1980**, *63*, 249. Beagley, B.; Pritchard, R. G. *Ibid.* **1982**, *84*, 129.

(36) ··· and at $p = 0.73$ and 0.77 with $|\delta| = 0.017°$, in the empty part of the scatterplot (Figure 9b).

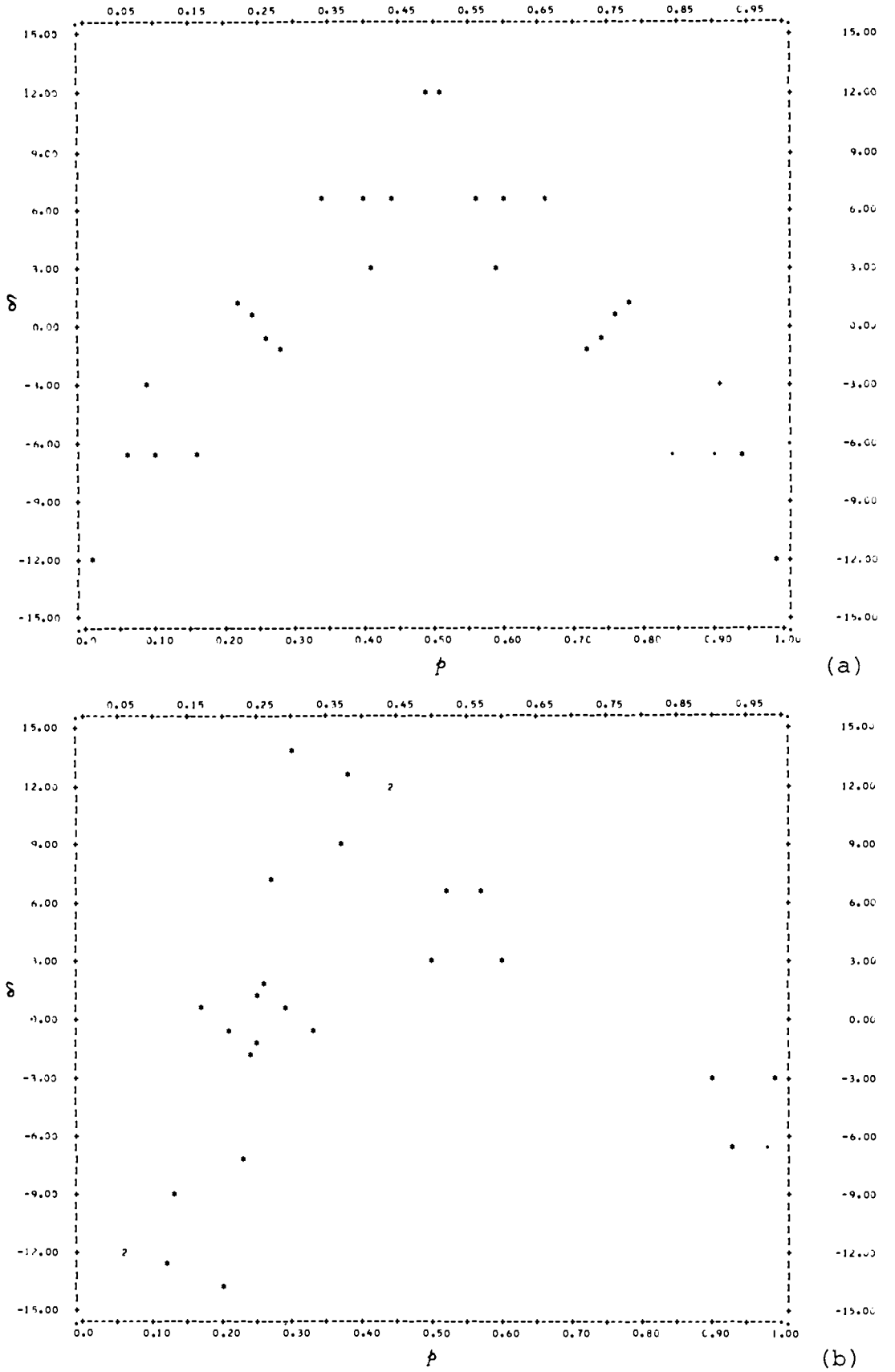

Figure 9. Scattergram of p vs. δ for (a) path 1 and (b) path 2 (prepared with program SPSS, ref 19).

conformations such as **16** are likely to be energetically unfavorable. It should be recalled here that the conformations with deviations from coplanarity also show misalignment of the PR_3 local threefold axes with respect to the M–P bond directions as discussed earlier.

The net effect of the distortions discussed so far can be gauged from the shortest C···C nonbonded distances between adjacent PR_3 groups. For cube 4′ in which the conformations resemble **11**, distances between atoms C21 and C33 range from 3.17 Å to 3.52 Å, for cube 2 with conformations resembling **2**, the shortest C···C distances are between 3.35 Å and 3.55 Å, and for cube 3 (1,5) with conformations resembling **3**, they are 3.44 Å to 3.63 Å. The shortest nonbonded distances are comparable to those

found between tertiary butyl groups in the highly crowded tri-*tert*-butylmethane.[37]

Scatterplots for α_{1M2} and α_{2M3} versus p were analyzed as well. It was not possible to discern a correlation. When the data points representing hydrides (X = H) were distinguished from the rest (X ≠ H), there was still no convincing trend of α_{iMj} vs. p; however, independently of p, α_{iMj} for the hydrides was always about 5° larger than α_{iMj} for the nonhydrides. The latter clustered in the range 97 ± 3°. Furthermore the hydrides (X = H) tend to show conformations like **2** or **11** ($p \sim 0.25$), whereas the nonhydrides are more evenly distributed. Both trends are compatible with the smaller size of H^- compared to that of other ligands X: Relatively small H–M–P angles are accompanied by relatively large P–M–P angles. This in turn makes relief of strain between PR_3 groups by nonplanar deformations less necessary; i.e., hydrides tend to prefer planar conformations ($p \sim 0.25$).

6. Discussion

In the preceding sections it was shown that the conformations of the PR_3 groups in molecules of the type $XM(PR_3)_3$ are highly correlated. There are two types of correlation: for one of them the changes in conformational angles of the PR_3 groups resemble gearing motion of interlocked cogwheels, for the other they resemble gearing motion to one side of the central PR_3 group and gear slippage to the other. All conformations show specific distortions from a reference model (ideal square-planar coordination of X and the PR_3 ligands to M as well as local, approximate threefold axes of PR_3 coincident with M–P bonds). First, the angles P1–M–P2 and P2–M–P3 are larger than 90° but seemingly insensitive to details of conformation. Second, the local threefold axes of $P1R_3$ and $P3R_3$ are tilted with respect to the corresponding M–P bonds by 5–7°, the R's being displaced toward X; the effect of this distortion is an opening of the R–P1–M and R–P3–M bond angles if R points toward P2, e.g., α_{13} in **2** and a closing of these angles if R points toward X, e.g., α_{32} in **2** (Figure 5). The misalignment of the local threefold axis of $P2R_3$ with respect to M–P2 depends on ω_2. For conformations that are mirror symmetric with respect to the XMP_3 plane (**2**) the local threefold deviates from M–P2 such as to open up the in-plane R–P–M angle (α_{21} in **2**) by ~3–7°. For conformations that are symmetric with respect to the XMQ plane, the $P2R_3$ group is tilted out of the XMP_3 plane by ~3–7° such that the unique R–P–M angle opens up (α_{23} in **1**). This tilt is accompanied by a deviation of the M–P2 bond itself from the mean molecular plane; the deviation amounts to ~9° and is to the same side as the tilt. The bonds M–P1 and M–P3 point to the opposite side of the mean molecular plane. In the case of the specially crowded triphenylphosphine complexes, the groups $P1R_3$ and $P3R_3$ also show a conformation-dependent tilting by 4–5°. This deformation again serves to either increase R–P–M angles if R points to $P2R_3$ (α_{13} in **2**) and to decrease them if R points toward X (α_{32} in **2**) or to accentuate the out of plane distortions of the M–P bonds (**1**). Taken together, the distortions from an idealized structural model all serve to increase the distance between neighboring PR_3 groups, i.e., to minimize nonbonded repulsions between them.

The conformational analysis summarized above has to be viewed against the background of early models in which phosphines were considered simply as rotationally symmetric cones characterized by a cone angle.[38] The inadequacy of this model has been recognized, and the phosphines have alternatively been considered as "irregular conic cogs" whose quantitative details are represented in so-called "ligand profiles".[39] Here we have not considered the detailed shape of the cogs because these are susceptible to changes; e.g., the phenyl conformations in PPh_3 change as the conformation of PR_3 itself changes.[40] Instead we have analyzed the *consequences* of the basic concept of cogwheels.

The concept of gears[41] and their description in terms of space group symmetry[42] have been introduced into conformational analysis of organic compounds elsewhere. For ditripticylmethane, (**18**), its derivatives, and similarly crowded molecules, the two-

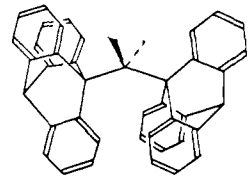

18

dimensional conformational map has been analyzed by molecular mechanics calculations,[42] temperature-dependent NMR experiments,[43] and scattergrams based on X-ray structural data.[44] In our context, the pertinent results from those studies are that molecular conformations observed in the solid state coincide with regions of low energy in the conformational map as calculated by molecular mechanics. The justification for our conclusions, namely that conformations like **1**, **2**, and **11** are energetically more favorable than **7** and **15**, thus rests on chemical analogy.

Taking the analogy one step further, we have to interpret the distribution of experimental structures in conformational space as a point-by-point mapping of the pathways followed by $XM(PR_3)_3$ molecules during dynamic conformational interconversions. Support for such interpretation would have to come, for example, from NMR experiments on appropriately labeled derivatives of $XM(PR_3)_3$ molecules at variable temperatures.[42,43] Short of such experiments we can say the following: None of the 15 structures shows a mirror symmetric conformation with P1 and P3 symmetry equivalent. On the other hand, all of the compounds for which NMR spectra are available show only one signal for P1 and P3.[45] Note that for each of the interconversion paths 1 and 2 the role (or environment) of P1 averaged over the full length of the path is identical with that of P3 averaged likewise; i.e., if the correlations found in the solid state are taken as a model for motion in solution they provide a rational explanation of the observed spectroscopic equivalence of P1 and P3.

Because of paucity of data it is impossible to say where along the pathway one would expect energy minima and transition states, nor is it possible to estimate activation energies. The occurrence of a red and an orange form of Wilkinson's catalyst,[12] $ClRh(PPh_3)_3$, indicates that differences in energy between different conformations are likely to be small: the main structural difference between the two molecules is in conformation. For the orange form $\{\omega_1, \omega_2, \omega_3\}$ are {13.4°, 68.4°, 111.0°} and for the red form {19.9°, 59.2°, 102.0°}. The changes are {6.5°, −9.2°, −9.0°}, corresponding to about 28% of the distance between mirror symmetric isoenergetic conformations like **10** and **3** (Figure 5b). The difference in molecular structure is due entirely to differences in molecular packing. This observation also sheds light on a recurring question: how relevant are crystal structure data to structure in solution? It would seem that the particular combination (ω_1, ω_2, ω_3) found in the solid state is probably not representative of the average structure in solution since it can take any set of values provided it is close to one of the pathways. On the other hand, solution conformations not close to either path, but falling into the empty regions of the scattergrams are very unlikely. In general, combinations of structural parameters associated with negligible differences in energy constitute a soft degree of freedom, and the particular combination observed in the solid state cannot be transferred reliably to solution structure.

(37) Bürgi, H. B.; Bartell, L. S. *J. Am. Chem. Soc.* **1972**, *94*, 5236.
(38) Tolman, C. A. *Chem. Rev.* **1977**, *77*, 313.
(39) Ferguson, G.; Roberts, P. J.; Alyea, E. C.; Khan, M. *Inorg. Chem.* **1978**, *17*, 2965.
(40) A preliminary analysis of these changes was inconclusive because of paucity of data.
(41) See, for example: Hounshell, W. D.; Iroff, L. D.; Iverson, D. J.; Wroczynski, R. J.; Mislow, K. *Isr. J. Chem.* **1980**, *20*, 65.
(42) Bürgi, H. B.; Hounshell, W. D.; Nachbar, R. B.; Mislow, K. *J. Am. Chem. Soc.* **1983**, *105*, 1427.
(43) Guenzi, A.; Johnson, C. A.; Cozzi, F.; Mislow, K. *J. Am. Chem. Soc.* **1983**, *105*, 1438.
(44) Johnson, C. A.; Guenzi, A.; Nachbar, R. B.; Blount, J. F.; Wennerström, O.; Mislow, K. *J. Am. Chem. Soc.* **1982**, *104*, 5163.
(45) See ref 4 and 7–10 for examples.

On the other hand, observations in the solid state for hard degrees of freedom are likely to be representative of solution structure as well.

It also seems worth noting that conformational analysis of a system as complex as $XM(PR_3)_3$ and with the amount of detail given above would be difficult to achieve by molecular mechanics calculations. The main difficulty is a lack of appropriate potential functions.

One might ask what conclusions can be drawn, from our analysis, about the catalytic activity of $ClRh(PPh_3)_3$[46] and related compounds. One possible answer would be: there are no direct conclusions, because, as has been shown in the last few years,[47] the catalytically active species is $ClRh(PPh_3)_2$ with one PPh_3 dissociated and not $ClRh(PPh_3)_3$. Another answer relates to catalysts for asymmetric hydrogenation[48] and related reactions. Consider the complexes **19** of chiraphos as an example. The basic asymmetry is located on the carbon atoms of the five-membered chelate ring. In order to induce asymmetry in hydrogenations, it must be transmitted to the opposite side of the Rh complex. It has been argued[49] that it is the phenyl groups on phosphorus that act as transmitters of asymmetry. Our analysis has certainly shown that it is possible to transmit information from one side of a Rh complex to the other ($P1R_3$ to $P3R_3$), that the mechanism of transmission may be based on nonbonded interactions, and that there is not necessarily a unique transmission of information (path 1 and path 2). So far we have not considered the role of the phenyl groups themselves, but it is known[2a] that triphenylphosphine shows certain preferred patterns of conformation. We are presently investigating how these patterns might combine with the conformation of the PR_3 groups in compounds of the type $XYM(PPh_3)_2$ and what the stereochemical consequences are if the two phosphine ligands are linked by an ethylene bridge as is the case for the ligand chiraphos (**19**).

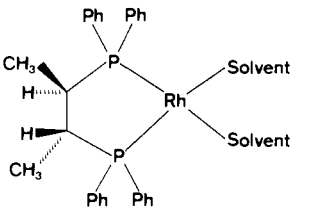

19

Acknowledgment. This work was supported by the Schweizerischer Nationalfonds zur Förderung der wissenschaftlichen Forschung.

Registry No. 1, 57810-25-0; **2**, 67426-13-5; **3**, 68664-86-8; **4**, 52242-35-0; **5**, 72778-75-7; **6**, 77700-88-0; **8**, 56954-48-4; **9**, 71357-03-4; **10**, 60364-00-3; **12**, 14694-95-2; **13**, 36103-64-7; **14**, 39248-25-4.

Supplementary Material Available: Appendix deriving eq 13 and 14 from eq 11 and 12 (5 pages). Ordering information is given on any current masthead page.

(46) Osborn, J. A.; Jardine, F. H.; Young, J. F.; Wilkinson, G. *J. Chem. Soc. A* **1966**, 1711.
(47) For a summary of the mechanism of catalysis see: Halpern, J. *Inorg. Chim. Acta* **1981**, *50*, 11.
(48) For a summary of the mechanism of asymmetric hydrogenation see: Halpern, J. *Science (Washington, D.C.)* **1982**, *217*, 401.
(49) Knowles, W. S.; Vineyard, B. D.; Sabacky, M. J.; Stults, B. R. In "Fundamental Research in Homogeneous Catalysis"; M. Tsutsui, Ed.; Plenum, New York, 1979; Vol. 3, 357.

Models for the Photosynthetic Water Oxidizing Enzyme. 2. Electronic, Magnetic, and EPR Characterization of a Binuclear Manganese(II) Semiquinone Complex

P. Mathur[†] and G. C. Dismukes*

Contribution from the Department of Chemistry, Princeton University, Princeton, New Jersey 08544. *Received May 3, 1982*

Abstract: The preparation and characterization of a tetranuclear manganese complex, $Mn_4(ASQ)_4(CO)_8$, and a binuclear complex into which it dissociates in solution, $Mn_2(ASQ)_4L_2$ (ASQ ≡ 2-acetyl-1,4-benzosemiquinone), is described. EPR spectroscopy and variable temperature magnetic susceptibility of the solution species indicate that there are two equivalent Mn(II) ions coupled by a ferromagnetic exchange interaction, having $J \geq 23$ cm^{-1}, fostered by two bridging semiquinones. This is evidenced by a paramagnetic ground state with a magnetic moment $\mu_{eff} = 6.78$, electron spin resonance fine structure consistent with an apparent spin $S = 3$ and having zero-field splitting parameters of $|D| = 0.103$ cm^{-1} and $|E| = 0.011$ cm^{-1}, a nearly isotropic 11-line hyperfine structure for ^{55}Mn with coupling constant $|A| = 45 \pm 3$ G, and a nearly isotropic $g = 2$. The quenching of the magnetic moment of the dimer with increasing temperature is interpreted to arise from the ferromagnetic coupling and, near room temperature, from an internal redox equilibrium in which $Mn_2(AQL)_4L_2$ and possibly $Mn_2(ASQ)_2(AQL)_2L_2$ (AQL ≡ 2-acetyl-1,4-benzoquinol dianion) form. This complex is discussed in relation to its suitability as a model for the magnetic properties of the photosynthetic water-oxidizing enzyme.

The mechanism by which green plats and algae oxidize water to molecular oxygen during photosynthesis is a poorly understood process. However, recent advances have established some clues on the identity of the active site of the metalloenzyme which mediates this important chemistry. This developing knowledge can now serve as a basis for the development of molecular models of the active site.[1,2]

EPR spectroscopic observation of the native enzyme in chloroplasts has shown that the active site consists of a binuclear, or possibly tetranuclear, manganese cluster.[3] Characterization of the manganese hyperfine structure, by comparison with mixed-valence binuclear Mn model compounds, has shown that Mn(III)

[†] Current Address: Ramjas College, Delhi University, Delhi, India.

(1) Cooper, S. R.; Dismukes, G. C.; Klein, M.; Calvin, M. *J. Am. Chem. Soc.* **1978**, *100*, 7248.
(2) Unni Nair, B. C.; Dismukes, G. C. *J. Am. Chem. Soc.* **1983**, *105*, 124.
(3) Dismukes, G. C.; Siderer, Y. *FEBS Lett.* **1980**, 121.

0002-7863/83/1505-7093$01.50/0